M4-5n development for the structural study of Charging Box Inclusion in Electrified Roads

Armelle Chabot

Armelle Chabot. M4-5n development for the structural study of Charging Box Inclusion in Electrified Roads. 24ème Congrès Français de Mécanique, Aug 2019, Brest, France. hal-02152820

HAL Id: hal-02152820
https://hal.science/hal-02152820

Submitted on 11 Jun 2019

M4-5n development for the structural study of Charging Box Inclusion in Electrified Roads

A. CHABOT[a]

a. IFSTTAR, MAST, CS5004, F-44344 Bouguenais Cedex, France, armelle.chabot@ifsttar.fr

Résumé :

Le rechargement dynamique des véhicules électriques par induction est possible en introduisant un boiter de recharge (CU) dans la route. Cependant, enfin d'anticiper les dégradations et d'étudier la durabilité des assemblages ainsi mis en jeu, il est nécessaire d'utiliser des outils de modélisations adaptés à l'étude de la fissuration d'interface entre deux milieux. Ce papier présente un développement effectué pour tenir compte d'un changement de matériaux au sein d'une ou plusieurs couches dans un outil de calcul dédié à l'analyse paramétrique des discontinuités dans les structures multicouches. L'exemple 2D d'une route électrifiée avec ou sans présence de fissure est illustré.

Abstract:

Electrified Roads (eRoad) that inductively charge in-speed the Electric Vehicles are a conceivable option through a Charging Unit (CU) introduced underneath the top bituminous layer of existing multilayered pavement structures. However, cracking and debonding phenomenon may occur between the CU and material layers. This phenomenon is one of the major distress parameters to consider for the durability of such new road concepts. This paper presents new developments done in an alternative modelling tool aiming to consider such inclusion and parametric calculations for future eRoad design. A 2D electrified road application case with or not a vertical crack is illustrated.

Mots clefs: Interface, multilayered structures, discontinuities, eRoad

1 Introduction

Under the objectives of the European Energy Agency to reduce the CO2 emissions for 2050, electrified Roads (eRoad) are proposed. Among all the proposed idea, one of them is to inductively charge the moving Electric Vehicle (EV). It leads to introduce Charging Units (CU) in one of the top layers of the existing multi-layered structures (Rim, 2013) (Chen *et al.*, 2015) (Pérez *et al.*, 2016). An additional thin layer is then placed to covert the all and to assure a good wheel/pavement contact (Figure 1). But due to severe different moving loads (depending on number of truck axles, speed, lateral wandering effect, etc.) and environmental conditions (temperature, water, freezing, etc), failures between the different materials involved may occur quickly (Petit and Chabot, 2017) (Buttlar *et al.*, 2018). Depending on the ratio of modulus between the different materials, cracking and debonding phenomenon between the CU and the structure is one of the major distress parameters to consider for

the durability of such new road concepts (Chabot and Deep, 2018). To first analyse the discontinuities in such composite structure, this paper presents a new development done in the dedicated 2D pavement tool, called M4-5nW (Nasser and Chabot, 2018). It aims to introduce the change of material (due to the CU location) in one (or several) layer(s) of such eRoad multi-layers. Then, a 2D electrified road application case with or not a vertical crack is illustrated.
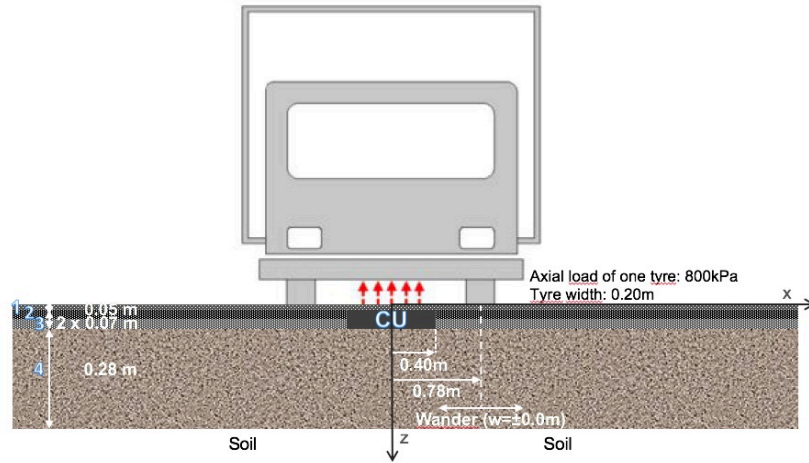

FIG. 1 - A half cross-sectional geometry of an eRoad with an inductive CU (After Chen *et al.*, 2019)

2   M4-5n development for an eRoad with a built-in CU

The M4-5nW tool is based on the M4-5n for the Multi-Particle Model of Multilayer Materials (M4) with 5n of equilibrium equations (n: total number of layers) and Winkler's Springs (W) for the half space soil. The M4-5n is specially designed to analyse the delamination of composite materials for multilayer bending problems (Chabot and Ehrlacher, 1998). The M4-5n can be viewed as a superimposition, following the vertical coordinate z, of n Reissner plates linked by shear stresses, $\tau_\alpha^{i,i+1}(x,y)$, and the normal stress, $v^{i,i+1}(x,y)$, at the interface between the consecutive layers i and i+1 (similarly i-1 and i, i ϵ {1,n-1}, α ϵ {1,2}) where h_i^+ and h_i^- are the coordinate of the higher and lower face of the layer i respectively (1).

$$\tau_\alpha^{i,i+1}(x,y) = \sigma_{\alpha 3}(x,y,h_i^+) = \sigma_{\alpha 3}(x,y,h_{i+1}^-)$$
$$v^{i,i+1}(x,y) = \sigma_{33}(x,y,h_i^+) = \sigma_{\alpha 3}(x,y,h_{i+1}^-)$$
(1)

This modelling reduces the real 3D problem to the determination of plane fields (x, y) per each layer i and at the interface i, i+1, (and i-1, i). Thus, the real 3D (2D) object is transforming into a 2D (1D) geometry. It allows convenient parametric calculations without singularity problems (Chabot and Ehrlacher, 1998) (Chabot *et al.*, 2013). Each i layer has its own behavioural laws, equilibrium equations and lateral boundary conditions. A vertical crack is easy to introduce into each layer separately (Chabot *et al.*, 2005).

In the so-called M4-5nW tool developed for 2D plane strain problems, the pavement is chosen equivalent to 3 material layers resting on a soil. The soil is assumed equivalent to a combination of a fictitious layer (shear soil layer) ensuring the transfer of shear stresses between the pavement multilayer and Winkler's Springs (W). In that case, a series of M4-5nW equation manipulations lead to the writing of a second-order differential system of twelve analytical equations depending only on one variable, "x" (Nasser and Chabot, 2018) (2).
.

$$AX''(x) + BX'(x) + CX(x) = DY^{0,1'}(x) + EY^{4,5'}(x) + FY^{0,1}(x) + GY^{4,5}(x)$$
(2)

The matrices $[A]_{12x12}$, $[B]_{12x12}$, $[C]_{12x12}$, $[D]_{12x2}$, $[E]_{12x2}$, $[F]_{12x2}$ and $[G]_{12x2}$ depend solely on the geometric and mechanical parameters of the equivalent elastic problem. The first order M4-5nW unknowns $U_1^i(x)$, $U_3^i(x)$ and $\phi^i(x)$ are, respectively, the average in-plane displacements, average out-of-plane displacements and average rotations of the layer i ($i \in [1,4]$) written as follows (3):

$$[\boldsymbol{X}] = \begin{bmatrix} X^1 \\ \vdots \\ X^n \end{bmatrix}_{3n \times 1} ; [X] = \begin{bmatrix} U_1^i \\ \phi_1^i \\ U_3^i \end{bmatrix} ; [Y^{0,1}] = \begin{bmatrix} \tau^{0,1} \\ v^{0,1} \end{bmatrix}_{2 \times 1} ; [Y^{n,n+1}] = \begin{bmatrix} \tau^{n,n+1} \\ v^{n,n+1} \end{bmatrix}_{2 \times 1} \quad i \in [1,4] \tag{3}$$

Following several previous works (Chabot *et al.*, 2005), the 2D tool solves semi-analytically the equations using the Newmark discretization (4).

$$\frac{X'_{j+1} + X'_j}{2} = \frac{X_{j+1} + X_j}{k_{j+1}} ; k_{j+1} = x(j+1) - x(j) \tag{4}$$

To test if the M4-5nW could be a convenient tool for the parametrical study of material inclusions in eRoads with possible macro cracks between materials, it is here proposed to analyse the elastic stress distribution around the charging box for the 2D plane strain example of Chen's PhD works (Chen *et al.*, 2015, 2019). Due to the symmetry of the problem, only the half cross geometry is studied (Figure 2). A "b" index notation, for the points of layers 2 and 3 containing the box inclusion, is used.
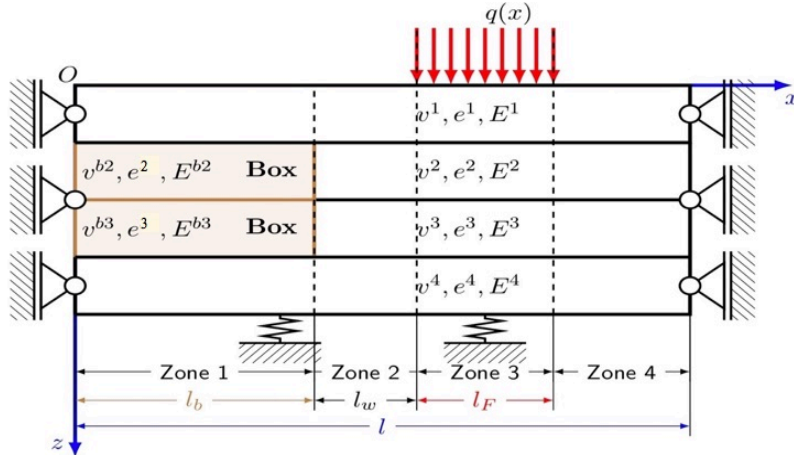

FIG. 2 - M4-5nW equivalent eRoad model of half the cross-sectional geometry (After Chabot and Deep, 2018)

In Zone 3 of Figure 2, the moving load q(x) describes the vertical and uniform load distribution from the tyre contact. The boundary condition at the upper interface (0,1 index) are then given in (5).

$$\begin{cases} \tau_1^{0,1}(x) = 0 \\ v^{0,1}(x) = q(x) \end{cases} \text{for } x \in [l_b + l_w, l_b + l_w + l_F] \tag{5}$$

Considering E^s, as the Young's modulus of the soil, the boundary condition at the bottom of the multilayer, interface 4,5 index, provides the connection between the shear layer and the Winkler foundation (with f, a correction factor, equal to 0.83 for a multilayer) (Nasser and Chabot, 2018) (6).

$$\begin{cases} \tau_1^{4,5}(x) = 0 \\ v^{4,5}(x) = -kU_3^4(x) \end{cases} \text{with } k = \frac{E^s}{h^*} \text{ and } h^* = \sum_{i=1}^{i=4} fe^i \sqrt[3]{\frac{E^i}{E^s}} \tag{6}$$

According to Chabot *et al.* (2005), the M4-5n boundary conditions at x=0 and x=l describing the fixed boundary on the both ends (Figure 2), are provided through equation (7):

$$\begin{cases} U_1^i(0) = U_1^i(l) = 0 \; ; \; \phi_1^i(0) = \phi_1^i(l) = 0 \\ \begin{cases} \phi_1^i 0 + U_{3,1}^i(0) + \dfrac{1+\vartheta^i}{5E^i}\left(\tau_1^{i-1,i}(0) + \tau_1^{i,i+1}(0)\right) = 0 \\ \phi_1^i(l) + U_{3,1}^i(l) + \dfrac{1+\vartheta^i}{5E^i}\left(\tau_1^{i-1,i}(l) + \tau_1^{i,i+1}(l)\right) = 0 \end{cases} \; ; \; i \in [1,4] \end{cases} \tag{7}$$

The Zone I, introduced in the M4-5nW tool, pertains to the CU location in layers nos. 2 and 3 of the structure (Figure 2). Since the CU box is made of a different material than the layer materials, the matrices of both Zone 1 ($x \in [0, l_b]$) and outside ($x \in [l_b, l]$)) differ (with the "b" index notation) in the second-order differential system function of the variable "x" (2). The continuity equations for displacement and rotations at ($x = l_b$) are then used according to equations (8), (9) and (10).

$$U_1^{2b}(l_b) = U_1^2(l_b) \text{ and } U_1^{3b}(l_b) = U_1^3(l_b) \tag{8}$$
$$U_3^{2b}(l_b) = U_3^2(l_b) \text{ and } U_3^{3b}(l_b) = U_3^3(l_b) \tag{9}$$
$$\phi_1^{2b}(l_b) = \phi_1^2(l_b) \text{ and } \phi_1^{3b}(l_b) = \phi_1^3(l_b) \tag{10}$$

The two interfacial behaviour relationships at interface i, i+1, as given in Equations (11) and (12) (Chabot and Ehrlacher, 1998), are then used to derive the continuity relationship between the two interfacial unknowns present due to the material discontinuity of the CU in layers 2 and 3.

$$\begin{aligned} \frac{e^{i+1}}{12} U_{3,1}^{i+1}(x) &+ \frac{e^i}{12} U_{3,1}^i(x) + U_1^{i+1}(x) - U_1^i(x) - \frac{5e^{i+1}}{12}\phi_1^{i+1}(x) - \frac{5e^i}{12}\phi_1^i(x) \\ &= -\frac{(1+v^i)e^i}{12E^i}\tau_1^{i-1,i}(x) - \frac{(1+v^{i+1})e^{i+1}}{12E^{i+1}}\tau_1^{i+1,i+2}(x) \\ &\quad + \left(\frac{(1+v^i)e^i}{4E^i} + \frac{(1+v^{i+1})e^{i+1}}{4E^{i+1}}\right)\tau_1^{i,i+1}(x) \end{aligned} \tag{11}$$

$$U_3^{i+1}(x) - U_3^i(x) = \frac{9}{70}\frac{e^i}{E^i}v^{i-1,i}(x) + \frac{9}{70}\frac{e^{i+1}}{E^{i+1}}v^{i+1,i+2}(x) + \frac{13}{35}\left(\frac{e^i}{E^i} + \frac{e^{i+1}}{E^{i+1}}\right)v^{i,i+1}(x) \tag{12}$$

In subtracting Equation (12) at point $x = l_b$ and using Equation (9), Equations (13) to (15) are obtained for the three interfaces affected by the presence of the CU (between layers 1 and 2, then between layers 2 and 3 and lastly between layers 3 and 4) (Figure 2).

$$\frac{13}{35}\left(\frac{e^1}{E^1} + \frac{e^2}{E^{b2}}\right)v^{b(1,2)}(l_b) + \frac{9}{70}\frac{e^2}{E^{b2}}v^{b(2,3)}(l_b) = \frac{13}{35}\left(\frac{e^1}{E^1} + \frac{e^2}{E^2}\right)v^{1,2}(l_b) + \frac{9}{70}\frac{e^2}{E^2}v^{2,3}(l_b) \tag{13}$$

$$\begin{aligned} \frac{9}{70}\frac{e^2}{E^{b2}}v^{b(1,2)}(l_b) &+ \frac{13}{35}\left(\frac{e^2}{E^{b2}} + \frac{e^3}{E^{b3}}\right)v^{b(2,3)}(l_b) + \frac{9}{70}\frac{e^3}{E^{b3}}v^{b(3,4)}(l_b) \\ &= \frac{9}{70}\frac{e^2}{E^2}v^{1,2}(l_b) + \frac{13}{35}\left(\frac{e^2}{E^2} + \frac{e^3}{E^3}\right)v^{2,3}(l_b) + \frac{9}{70}\frac{e^3}{E^3}v^{3,4}(xl_b) \end{aligned} \tag{14}$$

$$\frac{13}{35}\left(\frac{e^3}{E^{b3}} + \frac{e^4}{E^4}\right)v^{b(3,4)}(l_b) + \frac{9}{70}\frac{e^3}{E^{b3}}v^{b(2,3)}(l_b) = \frac{13}{35}\left(\frac{e^3}{E^3} + \frac{e^4}{E^4}\right)v^{3,4}(l_b) + \frac{9}{70}\frac{e^3}{E^3}v^{2,3}(l_b) \tag{15}$$

Similarly, by subtracting Equation (11), at $x = l_b$ and using Equations (8) to (10), a system of the three additional equations is obtained to assure the continuity of the interface shear stresses of the three interfaces involved. The system can thus be solved numerically given that all the boundary, continuity and interface conditions have been formulated and defined for this eRoad inclusion problem.

3   2D case results

To illustrate the results, the interfacial normal stresses are drawn for several elastic pavement structure cases (Figure 3). The load characteristics as well as the box dimension and layer thicknesses are given on Figure 1. The solutions are obtained using a uniform discretization (mesh width of 20mm) of the variable "x" and approximations around the changes of Zone 1 and 2 (Chabot and Deep, 2018). The soil model has been adapted with E^s=160MPa (6) and (E^4=270MPa, $\nu^4 = 0.35$) in order to fit Chen's result (Chen *et al.*, 2019). These equivalent soil values are kept for all the results presented here after. The prefabricated CU is supposed been made with a cement concrete material (E^{b2}=E^{b3}=30000MPa; $\nu^{b2} = \nu^{b3} = 0.25$) (Figure 2). For each case, a flexible pavement (purple curves with $\nu^1 = \nu^2 = \nu^3 = 0.35 \ and \ E^1 = E^2 = E^3$) with the assumption of the presence of a vertical crack between the CU and the layer is compared to a perfect bonded composite pavement made of a cement concrete for layers 1 and 2 with the same characteristic that the CU inclusion ($E^1 = E^2 = 30000$MPa, $\nu^1 = \nu^2 = 0.25$) casted on an asphalt layer with $E^3 \neq \ and \ \nu^3 = 0.35$.
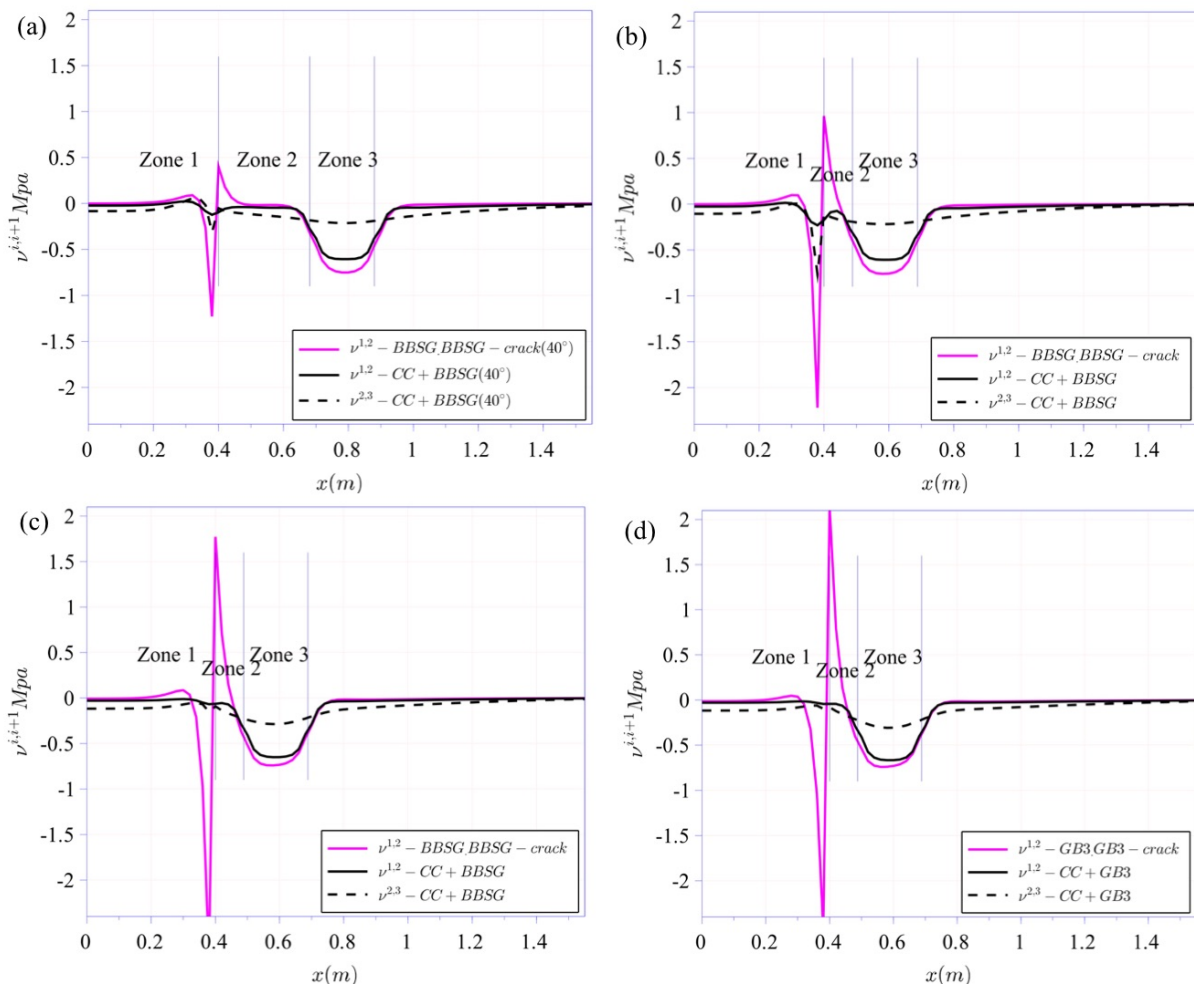

FIG. 3 - Interfacial normal stress comparison between the various cases: (a) BBSG ($40°, E^3 = 1000MPa$, w=0); (b) BBSG (40°, w=-0.2); (c) BBSG (15°C, w=-0.2) ; GB3 (15°C, w=-0.2)

Different combinations of materials are made in the aim to reduce the interfacial normal stress intensities between layers around the CU edge. Figures 3 (a) and (b) illustrate, whatever the pavement structural case is, that the closest the load is near to the box (for the lateral load position of "w" equal

to -0.2, see Figure1), the higher the intensity of the interfacial normal stresses are between layers 1 and 2. In addition, the highest the asphalt modulus of the flexible pavement is ($E^{BBSG\ (15°C)}$=5400MPa, $E^{GB3\ (15°C)}$=9300MPa), the highest the interfacial normal stress, between layers 1 and 2, is. Although it is reducing the ratio of modulus between layers 2 and 3 in case of the composite pavement structure.

4   Conclusion

In order to adapt pavement structures into eRoads with CUs that inductively charge the moving Electric Vehicle, pavement durable solutions in terms of material and structure need to be found. Due to change of materials between the inductive box inclusion and the layers, debonding phenomenon between those may occur quickly and under such condition, it is one of the major distress parameters to study for pavement structures. In that aim a new development that introduces material discontinuity in one or several layers have been done in an alternative modelling tool, called the M4-5nW. To contribute to this energy transition period, the tool offers quick parametric mechanical study possibilities.

Références

[1] W.G. Buttlar, A. Chabot, E.V. Dave, C. Petit, G. Tebaldi, State-of-the-Art Report of the RILEM Technical Committee 241-MCD Series Vol. 28, Springer International Publishing, 2018

[2] A. Chabot, A. Ehrlacher, Modèles Multiparticulaires des Matériaux Multicouches M4_5n et M4_(2n+1)M pour l'étude des effets de bord, JNC11, AMAC, France, 1998, 3, pp. 1389-1397

[3] A. Chabot, Q.D. Tran, A. Ehrlacher, A simplified modeling for cracked pavements / Modèle simplifié de chaussées fissurées, Bulletin des Labo. des Ponts et Chausses (258-259) (2005) 105-120.

[4] A. Chabot, M. Hun, F. Hammoum, Mechanical analysis of a mixed mode debonding test for composite pavements, Construction and Building Materials 40 (2013) 1076–1087.

[5] A. Chabot, P. Deep, 2D Multilayer Analysis of Electrified Roads with Charging Box Discontinuities, 13th ISAP Conference on Asphalt Pavements, Fortaleza, Ceará, Brazil, 2018

[6] F. Chen, N. Taylor, N. Kringos, Electrification of roads: Opportunities and challenges, Applied Energy 150 (2015) 109–119.

[7] F. Chen, R. Balieu, E. Córdoba, N. Kringos, Towards an understanding of the structural performance of future electrified roads: a finite element simulation study, International Journal of Pavement Engineering 20(2) (2019) 204-215.

[8] A. Chabot, C. Petit, Mechanisms of Cracking and Debonding in Pavements: debonding mechanisms in various interfaces between layers, Europ. J. of Env. & Civil Eng. 11(sup1) (2017) 1-2.

[9] T. M. Fisher, K. B. Farley, Y. Gao, H. Bai, Z. T. Tse, Electric vehicle wireless charging technology: a state-of-t-art review of magnetic coupling systems, Wireless Power Transfer 1(102) (2014) 87-96.

[10] H. Nasser, A. Chabot, A half-analytical elastic solution for 2D analysis of cracked pavements, Advances in Engineering Software 117 (2018) 107-122.

[11] S. Pérez, M. L. Nguyen, P. Hornych, E. Curran, Implementing recharging inductive technology on heavy-duty pavement bringing unlimited autonomy to electrical vehicles, Presented at the 8th Int. RILEM Conf. MCD2016, W3 : Roads of the future: towards durable and multi-functional infrastructures, Nantes, France, 2016 (https://mcd2016.sciencesconf.org/resource/page/id/15)

[12] C. T. Rim, The development and deployement of online electric vehicles (OLEV), Presented at the IEEE Energy Conversion Congress and Exposition (ECCE), Denver, CO, USA, 2013